Jump Phenomenon by Feedback Control of Flyback Converter

Takayuki HAMADA* Katsuhiko NISHIMURA* Kazuo KOBAYASHI*
Masatoshi NAKAHARA** Koosuke HARADA**

*Fujitsu Denso Ltd. Kawasaki, 213-8586 Japan
**Kumamoto Institute of Technology, Energy Electronics Laboratory.
Kumamoto, 860-0082 Japan

Abstract - Applying feedback control to a flyback converter in discontinuous conduction mode causes instability by a jump phenomenon under some snubber circuit conditions. In this paper, we clarify this jump phenomenon, analyze stability, and discuss circuit constants to avoid this jump phenomenon. We propose current-mode control without relying on circuit constants.

I. Introduction

These days, switching power supplies are commonly used. Many power supply units use switching regulators. A flyback converter is one type of switching regulator. It is made of simple circuitry and used as an insulated-type converter with a relatively small capacity. When used in the discontinuous conduction mode, the power factor of the flyback converter can be improved by using a commercial AC power supply for the input power of flyback converters that do not contain input capacitors. Feedback control can be stabilized by forming a first-order delay circuit. In such a setup, recovery characteristic of the rectifying diode does not generate so much noise. When the flyback converter is in the discontinuous conduction mode, however, feedback control, intended to stabilize the voltage and current of the flyback converter, may result in a jump phenomenon depending on the setting of the snubber circuit parameters [1] [2]. This is because the output does not increase monotonously with an increase in the conduction time resulting from PWM control. This condition occurs because after the energy of the reactor is released to the load, resonance occurs due to the main reactor and the sum of the stray capacitances in the main reactor, switch, and the capacitance of the snubber circuit.

This paper analyzes this phenomenon to find a region where no jump phenomenon occurs. It also describes a current mode feedback control that can avoid a jump phenomenon.

II. Circuit and Waveforms

Figure 1 shows the circuit used for analysis. In this circuit diagram, Ei, $\hat{e}_o$, L, Q, P, D, C, and R_L are the input voltage, the output voltage, the main reactor, the main switch, the pulse generator for driving the main switch, the rectifying diode, the smoothing capacitor, and the load resistance, respectively. Capacitor C_a and resistance R_a form a snubber circuit.

A transformer is used to isolate the input from the output. In this diagram, the transformer is represented by L and L_l (for the leakage inductance). The leakage inductance L_l causes a voltage surge when switch Q turns off. The snubber circuit is necessary to suppress this voltage surge. The capacitance C_a in the snubber circuit represents not only its own capacitance but also the stray capacitance in the switch and transformer.

Figure 2 shows the time chart of the switch Q, and the waveforms of the current i_2 through the reactor L and the voltage V_Q across the switch Q in a switching period T.

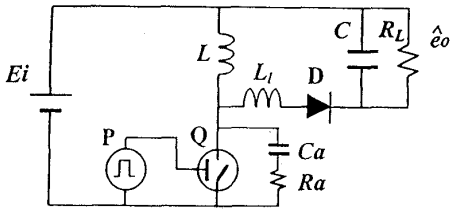

Figure 1: Circuit diagram of flyback converter.

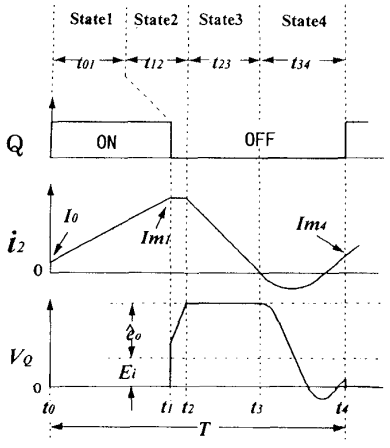

Figure 2: Waveforms of flyback converter.

0-7803-4489-8/98/$10.00 © 1998 IEEE

In State 1($t_0 \sim t_1$), switch Q is on to accumulate energy in reactor L. State 2($t_1 \sim t_2$) lasts from the time when switch Q turns off until the voltage V_Q becomes high enough for current to pass through diode D. In State 3($t_2 \sim t_3$), reactor L releases energy through diode D. In State 4($t_3 \sim t_4$), diode D is off to keep the series circuit comprised of L, C_a, and R_a in a damping oscillation.

In Figure 2, symbols $t_{01}, t_{12}, t_{23}, t_{34}$ denote the durations of the respective states. Symbol I_0 denotes the i_2 initial value (at t_0). Symbols Im_1 and Im_4 denote the i_2 value at t_1 and the i_2 value at t_4.

The internal resistances of reactor L, switch Q, and diode D are ignored to simplify the analysis. Reactor L_l requires a snubber circuit. However, L_l does not affect currents I_0 or Im_4 at t_0 or t_4 (discussed in this paper), because a surge caused by L_l in switch Q occurs just after t_2. Therefore, L_l is omitted.

Under the conditions stated above, current i_2 increases and decreases linearly in states 1 and 3, respectively. State 2 does not have much effect on this analysis, so we ignore it.

III. Equivalent Circuits and Equations for Each State

Figure 3 shows the equivalent circuits for states 1, 3, and 4 by assuming that switch Q and diode D operate ideally. The analysis described below uses an extended state space averaging method [3]. The current through $C_a \cdot R_a$, the current through diode D, and the voltage across C_a are denoted by i_1, i_d, and v_{c_a}, respectively. The voltage $\hat{e}_o$ across output capacitor C is also assumed to be a DC voltage source in the extended state space averaging method.

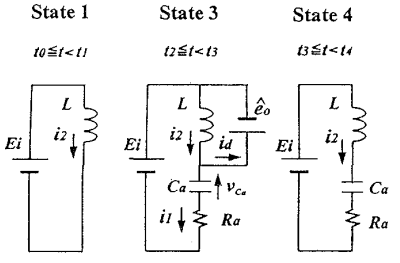

Figure 3: Equivalent circuits for each state.

A. State 1 ($t_0 \leqq t < t_1$)

Currents i_2 and Im_1 are given by

$$i_2 = I_0 + Ei \cdot t/L \quad (1)$$

$$Im_1 = I_0 + Ei \cdot t_1/L \quad (2)$$

B. State 3 ($t_2 \leqq t < t_3$)

Currents i_2, i_1, and i_d, and voltage v_{c_a} are given by

$$i_2 = Im_1 - \hat{e}_o \cdot t/L \quad (3)$$

$$v_{c_a} = (Ei + \hat{e}_o)(1 - e^{-t/(C_a R_a)}) \quad (4)$$

$$i_1 = \frac{Ei + \hat{e}_o}{R_a} e^{-t/(C_a R_a)} \quad (5)$$

$$i_d = i_2 - i_1 = Im_1 - \hat{e}_o \cdot t/L - \frac{Ei + \hat{e}_o}{R_a} e^{-t/(C_a R_a)} \quad (6)$$

Time t_{23} assume as following.

$$t_{23} \gg C_a R_a \quad (7)$$

Time t_{23} is obtained by assuming that Equation (6) equals zero.

$$i_d(t_{23}) = Im_1 - \hat{e}_o \cdot t_{23}/L = 0 \quad (8)$$

$$t_{23} = L \cdot Im_1/\hat{e}_o \quad (9)$$

Capacitor voltage $Vc3$ at time t_3 is given by

$$Vc3 = v_{c_a}(t_{23}) = (Ei + \hat{e}_o)(1 - e^{-t_{23}/(C_a R_a)}) \approx Ei + \hat{e}_o \quad (10)$$

C. State 4 ($t_3 \leqq t < t_4$)

Under the condition represented in Equation (7), current i_2 is approximated by

$$i_2 = e^{-at} \frac{Ei - Vc3}{L \cdot b} \sin(bt) \approx -e^{-at} \frac{\hat{e}_o}{L \cdot b} \sin(bt) \quad (11)$$

where

$$a = R_a/(2L), \quad b = \sqrt{1/(C_a L) - a^2} \quad (12)$$

Assuming that $1/(C_a L) - a^2 > 0$ with only the oscillation condition taken into account, current Im_4 is given by

$$Im_4 = i_2(T - t_3) = -\frac{\hat{e}_o}{L \cdot b} e^{-a(T - t_3)} \sin\{b(T - t_3)\} \quad (13)$$

IV. Relationship between the Load Resistance and the Output Voltage

This section describes how load resistance R_L and output voltage $\hat{e}_o$ are obtained. Figure 4 shows the output part of the flyback converter.

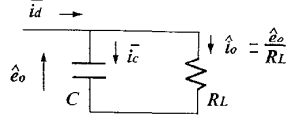

Figure 4: Output part of flyback converter.

The differential equation for the output voltage is represented using the extended state space averaging method as

$$\frac{d\hat{e}_o}{dt} = \frac{\bar{i}_c}{C} = \frac{\bar{i}_d}{C} - \frac{\hat{e}_o}{CR_L} \quad (14)$$

where $\bar{i}_c$ and $\hat{i}_o$ represent the capacitor current and the output current $\hat{i}_o = \hat{e}_o/R_L$, respectively. The symbol $^-$ in $\bar{i}_c$ and $\bar{i}_d$ indicates that they are averages.

From state 3, current $\bar{i}_d$ is obtained as

$$\bar{i}_d = \frac{1}{T}\{\frac{L \cdot Im_1^2}{2\hat{e}_o} - Ca(Ei + \hat{e}_o)\} \quad (15)$$

From Equation (14),

$$\frac{d\hat{e}_o}{dt} = \frac{\hat{e}_o}{C}[\frac{1}{T}\{\frac{L}{2}(\frac{Im_1}{\hat{e}_o})^2 - Ca(1+\frac{Ei}{\hat{e}_o})\} - \frac{1}{R_L}] \quad (16)$$

An equation to represent the relationship between t_1 and $\hat{e}_o$ is introduced. Equation (2) is divided by $\hat{e}_o$, and the resulting quotient is substituted into Equation (9) to obtain the relationship between time t_1 and $\hat{e}_o$:

$$t_3 = (1 + \frac{Ei}{\hat{e}_o})t_1 + \frac{L \cdot I_0}{\hat{e}_o} \quad (17)$$

where

$$X = \hat{e}_o/Ei \quad (18)$$

$$Y = L \cdot I_0/(T \cdot \hat{e}_o) \quad (19)$$

$$\begin{aligned} \alpha &= R_aT/(2L), \ \beta = \sqrt{1/(C_aL) - a^2} \cdot T \\ D_1 &= t_1/T, \ D_3 = t_3/T, \ p = T/\sqrt{LC} \\ q &= C_a/C, \ r = T/(CR_L) \end{aligned} \quad (20)$$

The substitution of Equations (18) and (19) into Equation (17) yields

$$D_3 = (1 + \frac{1}{X})D_1 + Y \quad (21)$$

To obtain a steady-state value, Equation (13) is assumed to be equal to I_0, and Equation (19) is used to yield

$$e^{-\alpha(1-D_3)}\sin\{\beta(1 - D_3)\} + \beta Y = 0 \quad (22)$$

The substitution of Equations (18), (19), and (20) into Equation (16) yields:

$$\frac{dX}{dt} = \frac{X}{T}\{\frac{p^2}{2}(Y + \frac{D_1}{X})^2 - q(1 + \frac{1}{X}) - r\} \quad (23)$$

Equations (21), (22), and (23) are the basic equations.

Since $dX/dt = 0$ in a steady-state,

$$\frac{p^2}{2}(Y + \frac{D_1}{X})^2 - q(1 + \frac{1}{X}) - r = 0 \quad (24)$$

Figure 5 shows the load current $\hat{i}_o$ vs. the output voltage $\hat{e}_o$ characteristics for R_a=10Ω and 1,000Ω. It is assumed that Ei=10V, L =1.5mH, C_a=5,000pF, T=50μs, and parameter t_1=20, 25, 30μs.

To clearly analyze this jump phenomenon, two R_a's with a large difference between them are used. One R_a is set to 10 Ω, which leads to a jump phenomenon occurring, and the other is set to 1,000 Ω, which prevents its occurrence. In addition, C_a is set to a value that nullifies the affect of stray capacitances in the switch and reactor and absorbs the surge voltage caused by leakage inductance L_l even when this inductance is relatively large (i.e. $L_l \approx 0.05L$).

In Figure 5, the region on the left-hand side of the dotted line represents the discontinuous conduction mode (DCM), and the one on the right-hand side indicates the continuous conduction mode (CCM).

As clearly shown in Figure 5 (a), in which points A and B are the intersections of the load line of R_L=1,000Ω with conduction time lines for t_1=25 or 30μs, the output voltage drops even when conduction time t_1 is increased from 25μs to 30μs. In Figure 5 (b), in which R_a=1,000Ω, this inversion does not occur.

To clarify this phenomenon, Figure 6 shows the relationship between the output voltage $\hat{e}_o$ and conduction time t_1 for R_L=1,000Ω. The large R_a causes $\hat{e}_o$ to increase monotonously as t_1 increases. Figure 7 shows the t_1 - $\hat{e}_o$ characteristics with the load resistance R_L as a parameter.

Figure 8 shows the Ei - $\hat{e}_o$ characteristics with t_1 as a parameter. As shown in the figure, the characteristics are linear with respect to the input voltage, but an inversion phenomenon has occurred in the output voltage even when t_1=30μs, which is greater than 25μs.

V. Jump Phenomenon

This section discusses a jump phenomenon caused by feedback when the output voltage $\hat{e}_o$ does not increase monotonously as the conduction time t_1 increases, as shown in Figure 5 (a) and in Figures 6 and 7.

A. Regulation mechanism and jump phenomenon [4]

Figure 9 (a) shows a regulation mechanism and a jump phenomenon similar to those in Figure 7 except that the horizontal scale represents the duty ratio and the vertical scale is enlarged. Figure 9 (a) assumes that the characteristic of the feedback control is linear. The feedback characteristic is given by

$$D_1 - D_0 = -K(\hat{e}_o - \hat{e}_{o0}) \quad (25)$$

where duty ratio D_0, output voltage $\hat{e}_{o0}$, and load resistance R_0 represent the respective reference operation point values, and K is the feedback gain. As the load resistance is made smaller than R_0, the output voltage $\hat{e}_{o0}$ drops and D_1 increases according to Equation (25). Just after the moment the

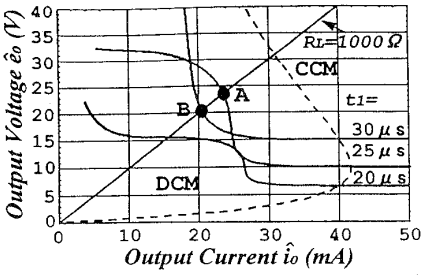

(a)

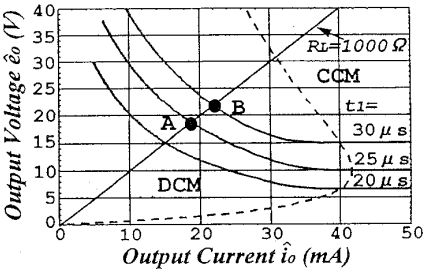

(b)

Figure 5: Load characteristics.
((a) R_a=10Ω, (b) R_a=1,000Ω)

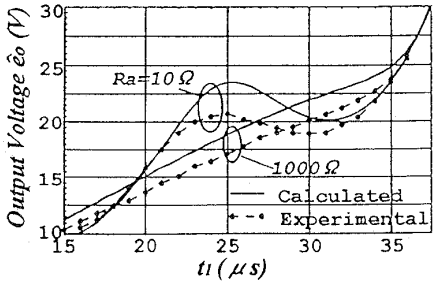

Figure 6: t_1 - $\hat{e}_o$ Characteristics. (R_L=1,000Ω)

load resistance becomes smaller than R_1, that is, at point P_1, the duty ratio becomes D_a and a jump occurs to point P_2. When the load resistance is further decreased to R_3 at point P_3, a jump occurs to point P_4. When the load resistance is R_4, the operation point reaches at point P_5.

On the contrary, when the load resistance is increased from R_4, a jump occurs from point P_6 to point P_7 at R_2. When it is further increased to R_0, a jump occurs from point P_8 to point P_0.

Figure 9 (b) represents this trajectory as the load current $\hat{i}_o$ vs. the output voltage $\hat{e}_o$ characteristics. Figure 9 (a) assumes R_0=4,550Ω, R_1=3,250Ω, R_2=875Ω, R_3=790Ω, R_4=600Ω, and K=0.12. Both the calculated values and the experimental results are plotted. The differences between the calculated and experimental values may be due to the fact that no circuit loss was included in the calculations.

B. Stability analysis using small-signal

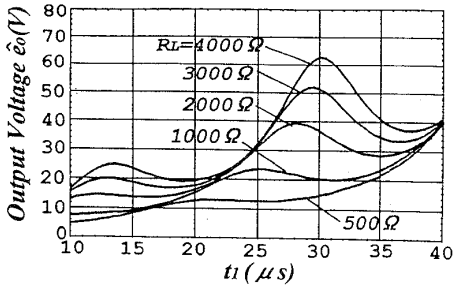

Figure 7: t_1 - $\hat{e}_o$ Characteristics. (R_a=10Ω)

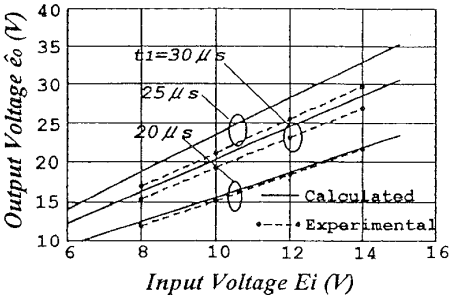

Figure 8: Ei - $\hat{e}_o$ Characteristics.
(R_a=10Ω, R_L=1,000Ω)

model

Let us consider the small-signal model for Equations (21), (22), and (23), that is the duty ratio $D_1 \rightarrow D_1 s + \Delta D_1$ and the voltage conversion ratio $X \rightarrow Xs + \Delta X$, where the suffix s represents a steady-state value. The substitution of these values into Equation (23) yields

$$\frac{d(\Delta X)}{dt} = \frac{Xs}{T}p^2\left(Ys + \frac{D_1 s}{Xs}\right)\Delta Y + \frac{p^2}{T}\left(Ys + \frac{D_1 s}{Xs}\right)\Delta D_1 + \frac{1}{TXs}\left\{-p^2\left(Ys + \frac{D_1 s}{Xs}\right)D_1 s + q\right\}\Delta X \quad (26)$$

From Equation (21),

$$\Delta D_3 = -\frac{D_1 s}{Xs^2}\Delta X + \left(1 + \frac{1}{Xs}\right)\Delta D_1 + \Delta Y \quad (27)$$

From Equation (22),

$$\{\alpha e^{-\alpha(1-D_3 s)}\sin\beta(1-D_3 s) - \beta e^{-\alpha(1-D_3 s)}\cos\beta(1-D_3 s)\}\Delta D_3 + \beta\Delta Y = 0$$

$$\therefore \quad f\Delta D_3 + \beta\Delta Y = 0 \quad (28)$$

where f is given by

$$f = e^{-\alpha(1-D_3 s)}[\alpha\sin\{\beta(1-D_3 s)\} - \beta\cos\{\beta(1-D_3 s)\}]$$

From Equations (27) and (28),

$$\Delta Y = \frac{1}{1+\beta/f}\left\{\frac{D_1 s}{Xs^2}\Delta X - \left(1 + \frac{1}{Xs}\right)\Delta D_1\right\} \quad (29)$$

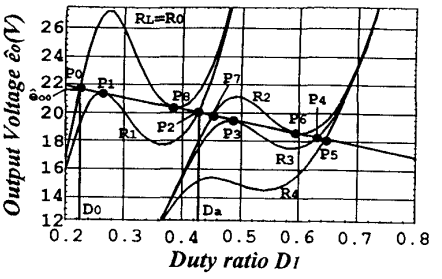

(a) D uty ratio - output voltage.

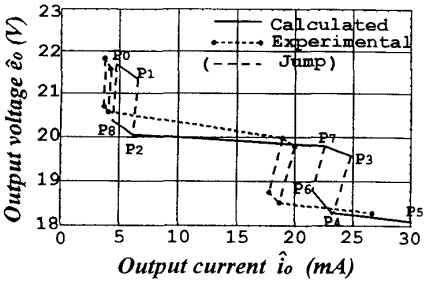

(b) Load characteristics.

Figure 9: Regulation mechanism.

Substituting Equation (29) into Equation (26) yields

$$\frac{d(\Delta X)}{dt} = [\frac{1}{TXs}\{-p^2(Ys+\frac{D_1 s}{Xs})D_1 s + q\} + \frac{Xs}{T}p^2(Ys+\frac{D_1 s}{Xs})\frac{1}{1+\beta/f}\frac{D_1 s}{Xs^2}]\Delta X + [\frac{p^2}{T}(Ys+\frac{D_1 s}{Xs}) - \frac{Xs}{T}p^2(Ys+\frac{D_1 s}{Xs}) \cdot \frac{1}{1+\beta/f}(1+\frac{1}{Xs})]\Delta D_1 \quad (30)$$

Let g and h be the coefficients of ΔX and ΔD_1, respectively, to yield

$$g = \frac{1}{TXs}\{-\frac{p^2\beta D_1 s}{\beta+f}(Ys+\frac{D_1 s}{Xs}) + q\} \quad (31)$$

$$h = \frac{p^2}{(\beta+f)T}(Ys+\frac{D_1 s}{Xs})(\beta - fXs) \quad (32)$$

Thus, Equation (30) is changed to

$$\therefore \quad \frac{d(\Delta X)}{dt} = g\Delta X + h\Delta D_1 \quad (33)$$

Applying a Laplace transform to this equation yields

$$s\Delta X^* = g\Delta X^* + h\Delta D_1^* \quad (34)$$

where * represents the Laplace transform.
Let us define a transfer function as $Gc \equiv \Delta X^*/\Delta D_1^*$. Thus,

$$Gc = h/(s-g) \quad (35)$$

Let us define the feedback characteristic as

$$\Delta D_1^* = -K'\Delta X^* \quad (36)$$

where $K' = E_i K$. The transfer function at the feedback is given by

$$G_{CF} = \frac{G_C}{1+K'G_C} = \frac{h/(s-g)}{1+K'h/(s-g)} = \frac{h}{s-(g-K'h)} \quad (37)$$

Thus, the pole of G_{CF} is given by $g_F = g - K'h$. The operation remains stable as long as g_F is negative. When g_F becomes positive, a jump phenomenon occurs.

Here, the output voltage is stable when $h \geq 0$ because $h \geq g/K'$ and K' is large enough for practical use.

Assuming h=0 for Equation (32), substituting Equations (18) to (20) into Equation (32) yields

$$\frac{\hat{e}_o}{L\cdot b}e^{-at}\{a\sin(bt) - b\cos(bt)\} = \frac{Ei}{L} \quad (38)$$

The left-hand side of Equation (38) expresses the result of differentiating current i_2 in Equation (11) with respect to time t. Because the voltage across the reactor L is $L \cdot di_2/dt$, multiplying L each side of Equation (38) yields

$$\frac{\hat{e}_o}{b}e^{-at}\{a\sin(bt) - b\cos(bt)\} = Ei \quad (39)$$

The left-hand side of this equation represents the voltage across reactor L between times t_3 and t_4. The right-hand side represents the input voltage. Equation (39) reveals that the jump phenomenon is prevented when the voltage V_Q across the switch is positive in state 4 (t_3 to t_4).

Figure 10 shows the relationship between the normalized output voltage $\hat{e}_o$ and the normalized resistance R_a in Equation (39). In this Figure 10, the circuit parameters of the experimental values are t_1=25μs, T=50μs, L=1.5mH, and C_a=5,000pF, that is $\sqrt{L/C_a} \approx 0.55 \times 10^3$.

The reasons for the difference between the calculated and experimental values in this figure is explained as follows. First is that the iron loss of main reactor L is not considered in the calculated value. Second is that the initial voltage value V_C3 of C_a in state 4 is estimated to be $E_i + \hat{e}_o$ in Equation (10) by Equation (7). However, when the voltage conversion ratio is high, state 4 starts without a complete charge of $E_i + \hat{e}_o$ by the time constant $C_a R_a$. Therefore, the actual value is smaller than $E_i + \hat{e}_o$.

The analysis and experiments reported in this paper have all been based on the following application.

A DC/DC converter for a telecommunication power supply uses a bipolar transistor. The bipolar transistor can drive the main switch at a low voltage, it does not have a body diode, and it can operate with an inverse collector-emitter voltage. This DC/DC converter is a boost-type converter that uses a low-input voltage.

These days, however, field effect transistors FETs are used in main switches. In this case, no inversion occurs in the relationship between the conduction time t_1 and the output voltage $\hat{e}_o$, as shown in Figure 7. The output voltage $\hat{e}_o$ remains constant against an increase in conduction time t_1 as long as the body diode of the FET is on. However, when the feedback gain is high, the feedback control becomes unstable.

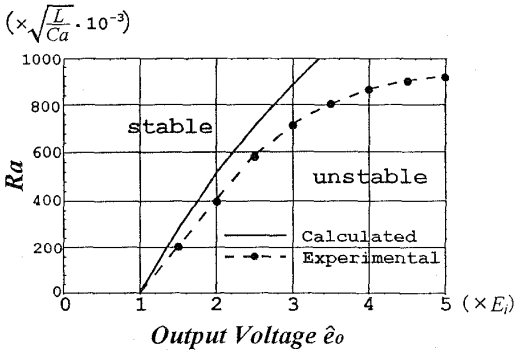

Figure 10: Limit of R_a.
(Experimental : E_i=10V, L=1.5mH, C_a=5,000pF, t_1=25μs, T=50μs)

VI. Current Mode Control Feedback

Figure 12 shows a current mode control feedback scheme: a method to avoid the jump phenomenon, as described earlier. Figure 11 show the Im_1 - $\hat{e}_o$ characteristic while Figure 6 show the t_1 - $\hat{e}_o$ characteristic. The characteristics have an almost constant slope regardless of whether R_a is 10Ω or 1,000Ω. The characteristics of calculated and experimental values agree well, and $\hat{e}_o$ increases monotonously with Im_1.

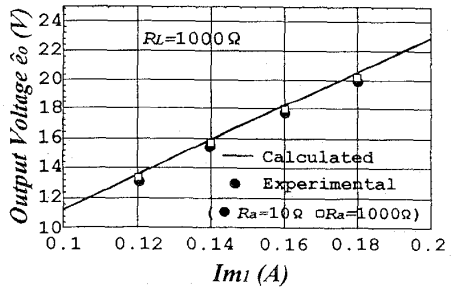

Figure 11: Im_1 - $\hat{e}_o$ characteristics.

As shown in Figure 12, the error amplifier (Error AMP) compares voltage $\hat{e}_o$ with reference voltage (V_{ref}) and amplifies the difference. The detector resistance R_d detects Im_1, and the comparator (PWM COMP) determines Im_1. The output voltage $\hat{e}_o$ is fed back via Im_1. Thus, current mode control feedback is realized. The relationship between $\hat{e}_o$ and Im_1 for the feedback constant K'' is given by

$$Im_1 - Im_{10} = -K''(\hat{e}_o - \hat{e}_{o0}) \qquad (40)$$

where Im_{10} and $\hat{e}_{o0}$ correspond to the reference operation points. The output energy generated with Im_1 is given by

$$\frac{L \cdot Im_1^2}{2T} = \frac{\hat{e}_o^2}{R_L} \qquad (41)$$

Figure 13 shows the load characteristic obtained by evaluating Equations (40) and (41) with the maximum Im_1 = 0.15 A, K'' = 0.1, Im_{10} = 0.1 A, $\hat{e}_{o0}$ = 20 V, and L = 1.5 mH. The results of the experiment are also shown. The output current $\hat{i}_o$ drops near 17 mA because Im_1 is limited to a maximum of 0.15 A. The stability of the output voltage varies according to the set value of constant K''. In Figure 13, it is set to 0.1 for comparison with Figure 9 (b).

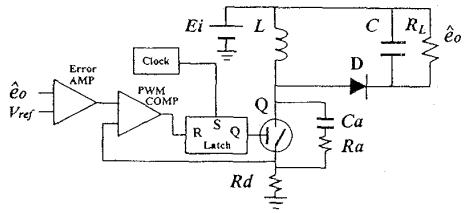

Figure 12: Circuit diagram of current mode control.

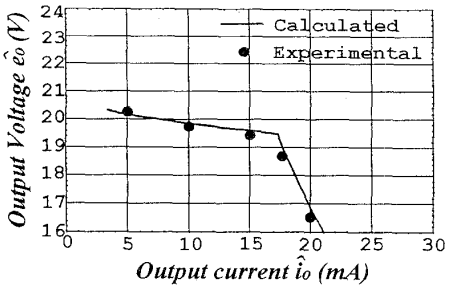

Figure 13: Load characteristics of current mode control. (R_a =10Ω)

VII. Experimental Results

The t_1 - $\hat{e}_o$ and the E_i - $\hat{e}_o$ characteristics as obtained from the experiment are shown in Figures 6 and 8, respectively.

We have successfully proven that a region exists in which output voltage $\hat{e}_o$ does not increase when conduction time t_1 increases, as shown in Figure 6. In Figure 8, the relationship between the output

voltage $\hat{e}_o$ and the conduction time t_1 is inverted when t_1=25μs and 30μs. With this characteristic, applying feedback makes the output voltage unstable, because a jump phenomenon occurs as shown in Figure 9 (b). Figure 11 shows the Im_1 - $\hat{e}_o$ characteristics for current mode control feedback. Figure 13 is the result of an experiment made with this feedback method. As shown in this figure, there is no jump phenomenon in this control. In Figures 6, 8, and 9 (b), the differences between the calculated and experimental values may be due to the fact that no circuit loss was included in the calculations. For reference, Figure 14 shows a waveform observed at point A in Figure 5 (a), where output voltage $\hat{e}_o$ begins to decrease with an increase in conduction time t_1.

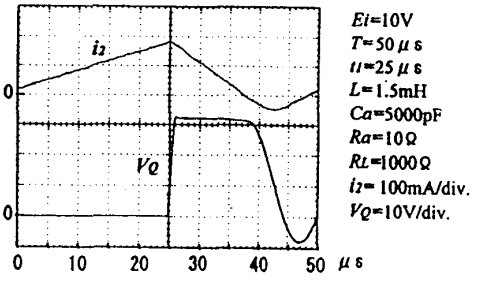

Figure 14: Waveforms of i_2 and V_Q.

VIII. Conclusion

A condition for the jump phenomenon exists in the flyback converter with the conduction time feedback control. We clarified this phenomenon by investigating a regulation mechanism and analyzed the stability of the output voltage by a small-signal model to find a region where no jump phenomenon occurs.

We found that the jump phenomenon occurs in a discontinuous conduction mode when $\hat{e}_o > Ei$ and switch voltage $V_Q < 0$. This was demonstrated in our experiments.

We have also found that no jump phenomenon occurs in a current mode control converter where the peak value of the reactor current is controlled, regardless of the snubber circuit's parameters.

This analysis is applicable to other types of converters.

References

[1] K.Kobayashi, K.Nishimura, T.Ookuma, and T.Niikura, "Consideration of the Instability of Flyback Converter," Society Conference of The Institute of Electronic Information and Telecommunication, B-916, p.401, 1996.

[2] K.Kobayashi, K.Nishimura, and T.Hamada, "Unstable Analysis of Flyback Converter in Discontinuous Conduction Mode," IEICE Tech. Report, EE97-69, pp.37-43, Feb. 1998.

[3] T.Ninomiya, M.Nakahara, T.Higashi, and K.Harada, "Unified Analysis Method for Resonant Converters, " Papers of The Institute of Electronic Information and Telecommunication, B-1, Vol.J72-B-1, No.10, pp.857-867, Oct. 1989.

[4] T.Ninomiya, K.Harada, and M.Nakahara, "Analysis of the Stability of Step-up and down DC-DC Converters, " Journal of The Institute of Electronic Telecommunication, Vol.J66-C, No.1, pp.1-8, Jan. 1983.